NUMERICAL ANALYSIS OF FILM SQUEEZE FOR A STEPPED PIN IMMERSED IN A NEWTONIAN FLUID

Alex-Florian CRISTEA[1], Daniela COBLAŞ[2]

Lucrarea prezintă analiza numerică a mişcării de expulzare a unui fluid Newtonian într-o geometrie cilindru cu treaptă. Simulările numerice au fost realizate pentru mişcarea de expulzare cu viteză constantă şi pentru mişcarea oscilatorie de expulzare, folosind o soluţie nestaţionară (discretizare spaţială deformabilă), pentru două grosimi iniţiale ale filmului fluid şi diferite viteze de expulzare. Prezenţa pragului conduce la mutarea centrului de presiune către zona cu grosime mică de film şi la apariţia unor viteze mari de curgere în zona treptei. În cazul mişcării oscilatorii de expulzare, variaţia forţei normale în timp, neglijând fenomenele cavitaţionale, nu prezintă o formă sinusoidală (conform profilului de deplasare impus) depinzând de viteza de curgere şi de grosimea filmului fluid. Lucrarea este de interes practic in cazul pompelor cu pistoane axiale, sau pentru lagărele axiale a turbinelor hidrodinamice.

The paper presents a 3D transient numerical analysis of the squeeze-film flow of a Newtonian fluid for stepped pin geometry. The numerical simulations have been performed with a commercial code, considering constant and sine-wave profile velocity squeeze. The analysis covered broad range of squeeze velocities and a couple initial film thicknesses. The step shifted the maximum pressure towards the minimum film thickness zone, and accelerated the flow near the step. For a sine-wave displacement of the surfaces, the resulting thrust neglecting cavitational effects follows more closely the velocity profile than the surface displacement profile, though it depends on both. The paper presents interest also in practical applications as axial piston pumps and thrust bearings of the hydraulic turbines.

Keywords: squeeze film, stepped pin, Newtonian fluid, CFD

1. Introduction

The majority of machine elements associated with relative motion contain a thin layer of lubricant sandwiched between solid surfaces. This reduces friction and increases components lifetime. Solid surfaces are separated as long as a pressure build-up mechanism exists within the film to support the loads. The most

[1] PhD Sudent, Machine Elements and Tribology Department, University POLITEHNICA of Bucharest, Romania, acristea@omtr.pub.ro
[2] PhD, Hydraulics, Fluid Machinery and Environmental Engineering Department, University POLITEHNICA of Bucharest, Romania

important mechanisms [1] are the "physical wedge", where a convergent gap is created between two surfaces in relative motion, and "squeeze-film flow", where fluid is expelled as surfaces approach each other. A viscous fluid between solid or viscoelastic surfaces provides support and cushioning for machinery [2]. Squeeze-film dampers are special elements that enable shock and vibration damping [2-3].

Analytical modeling of squeeze-film flow is not a simple task; even when hydrodynamic lubrication simplifications [1-4] are considered, solutions are limited to parallel-plate configurations, and are inaccurate around corners. Real fluids contain microscopic gas bubbles that under cyclic loading coalesce and lead to cavitation and film rupture under reverse squeeze [4]. Film rupture is not simple to model, as bubble parameters and surface tension have to be considered.

Squeeze-film flow concerns engineering, rheology and biology [5-7]. From the engineering point of view, the squeeze processes occur frequently in machine elements. An example is when the surface defects are comparable to the film thickness. For a convergent runner-pad with runout, squeeze can alter the thrust and drag generated through physical wedge.

Though the runner-pads with runout performance depends on both pressure build-up mechanisms, only the squeeze-film flow effects are considered in a first stage analysis, and represents the topic of the current paper.

The present paper presents a CFD 3D transient theoretical analysis of isothermal-isoviscous incompressible squeeze-film flow of a stepped pin fully immersed in a high viscosity Newtonian fluid. The solution is obtained with the ANSYS Fluent commercial software [8] for constant velocity and sine-profile velocity squeeze and considering a couple of initial film thicknesses.

2. Computational domain and simulation parameters

Film squeeze has been studied for a stepped pin with a diameter $d = 4\ mm$ and step $s = 20\ \mu m$, cross-section at symmetry plane in Fig. 1. Two initial minimum film thicknesses have been considered, i.e. $h_0 = 20\ \mu m$ and $40\ \mu m$. For constant velocity squeeze film flow, simulations at lower initial film thicknesses represented a prolongation of the higher initial film thicknesses. Though an increase of the simulation time would have produced similar results, the two initial film thicknesses method has been preferred to reduce calculations time.

If the lower surface travelled sideways towards the gap, hence creating a "physical wedge", then the geometry would have corresponded to a classical Rayleigh step [9]. Additional information on the "physical wedge" analysis of a Rayleigh stepped pin, including a theoretical model and experimental evidence, can be found in reference [9].

For the study presented herein, runout has been associated with a vertical travel of the entire lower surface, leading to squeeze-film flow. Though surface

tilt has not been considered, the 3D stepped pin has not been previously analyzed in squeeze-film flow studies. The case is representative for a stationary pin and a travelling lower surface of relatively larger extent, or a stationary machine element sandwiching a fluid with its surfaces approaching one another.

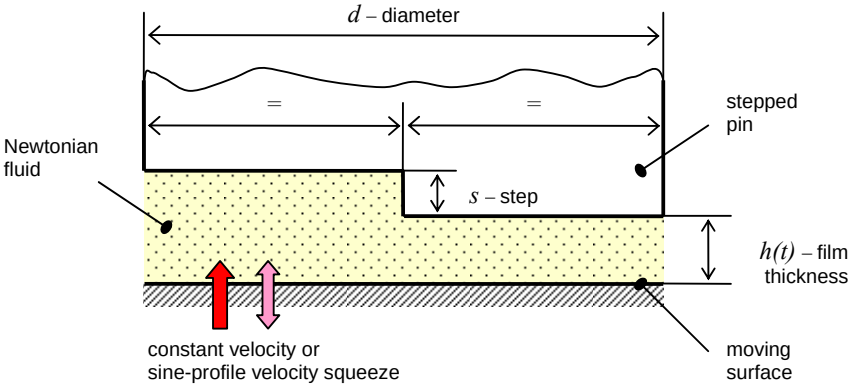

Fig. 1. Stepped pin cross-section (clearance exaggerated).

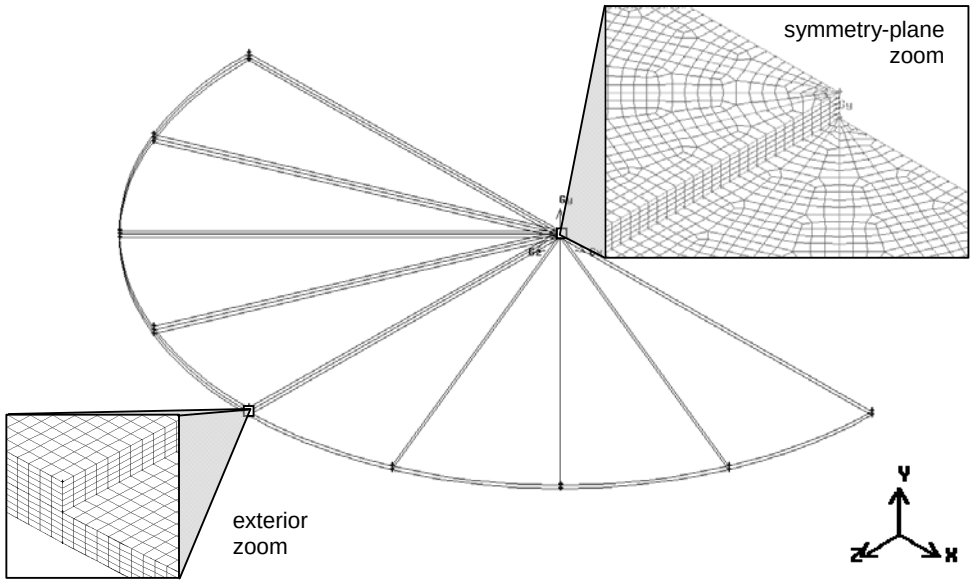

Fig. 2. Computational domain (overview and zoom) for the fluid film represented with initial minimum film thickness $h_0 = 20\ \mu m$.

The volume of fluid squeezed between the upper and lower surfaces represented the computational domain, Fig. 2. As the pin is symmetrical, just one half has been sufficient to characterize its performance. A finite volume approach has been chosen with a structured grid, made from 8-node hexahedron cells of $\Delta x \approx \Delta z \approx 8\ \mu m$ and $\Delta y = 4\ \mu m$ average size. A deformable mesh with layering enabled allowed Δy for the cells next to the bottom wall to decrease under squeeze. Cell sizing and *x-z* layout were maintained at both computational domains, i.e. $h_0 = 20\ \mu m$ and $h_0 = 40\ \mu m$.

The computational domain has been partitioned to speed-up calculations on multi-core and / or multi-processor systems. A typical problem that appears in lubrication simulations is the cell aspect ratio due to the small film thickness compared to the other dimensions. As a dimensionless approach that remapped the computational domain could not be implemented in Fluent, the problem was addressed by increasing the number of cells on *x* and *z*.

The solution has been derived with the Fluent pressure-based parallel solver [8] considering Green-Gauss cell based gradient approximation. A standard pressure discretisation was chosen, while QUICK was preferred for the momentum equations. As the solution required a transient analysis, pressure-velocity coupling has been done through the PISO algorithm. The Newtonian lubricant was considered isoviscous, with dynamic viscosity $\mu = 10.25\ Pa.s$ – a typical value for viscous silicone oils, and at constant temperature. The computational domain has been regarded to be completely filled with lubricant, with no gas or air bubbles within. Therefore, the model considered a constant contact area. No slip boundary conditions have been imposed at the upper and lower surfaces; the lateral surfaces have been treated as pressure outlets.

When the surfaces are not fully immersed in lubricant, such as the case of parallel disk rheometers, one may consult the review paper [7].

At constant velocity squeeze, the lower surface was moved towards the upper surface sequentially with a total $\Delta h = 4\ \mu m$, at various speeds $v = 1,\ 10^{-1},\ 10^{-2}$ & $10^{-3}\ mm/s$. For sine-profile squeeze, the surface movement amplitude was $A = 4\ \mu m$ in both directions, the frequencies $\omega = 0.25,\ 2.5,\ 25$ & $250\ Hz$ with the corresponding periods $T = 4,\ 0.4,\ 0.04,\ 0.004\ s$. Three periods have been simulated for each of the sine-profile cases. Motion profiles with the lower surface position at discrete time steps have been made prior to the simulations, and loaded into Fluent to manage with the deformable mesh. The squeeze velocity resulted from shifting the surface between consecutive time intervals. An analysis of time step and convergence criteria influence on the results has been done for a test case before all simulations started.

Although a commercial software package was used for the study presented herein, the problem can be solved with "in-house" codes based on Navier-Stokes algorithms [10]. A simpler approach to the Navier-Stokes solution represents the

Reynolds equation approach, widely used in lubrication. A comparative study [11] between the Navier-Stokes and Reynolds equation based solutions for a *2-D* physical wedge Rayleigh step revealed that overall performance parameters show excellent agreement, however localized errors near the step are to be encountered.

3. Results and discussion

Reducing the *3-D* computational domain to half of the stepped pin, Fig. 2, enabled performing more accurate simulations than the full pin with the existing computational hardware by using refined meshes. For this reason, global parameters, such as the thrust presented in this section must be doubled when considering the total pin. However, local parameters such as cell pressure or face velocity do not require additional data processing.

For constant velocity squeeze-film flow, Fig. 3, more thrust was generated at lower film thicknesses; hence, a decrease to approximately half of the minimum film thickness had the same effect as increasing squeeze velocity with one order of magnitude. For the geometry and fluid considered, thrust values can be considered high at *1 mm/s*.

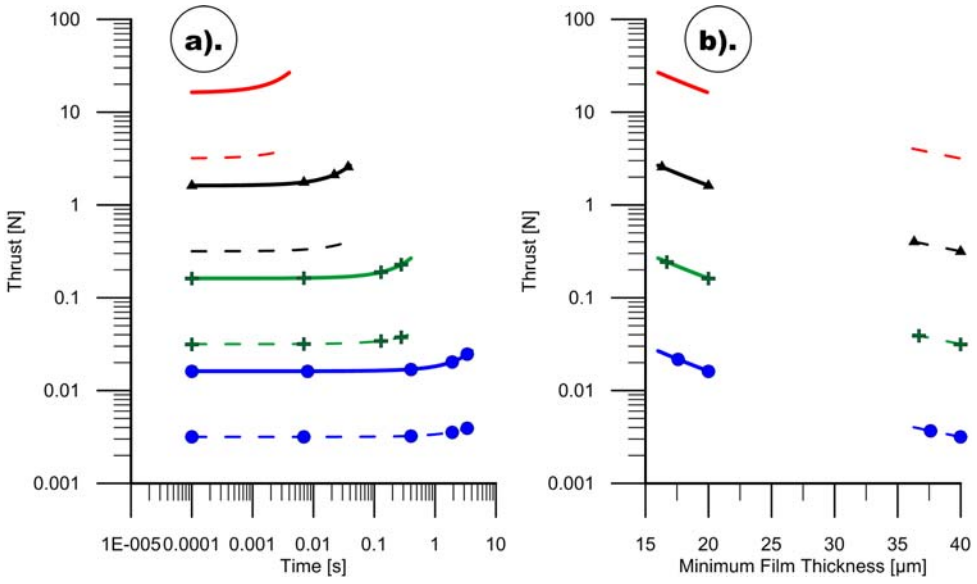

Fig. 3. Theoretical thrust generated at constant velocity squeeze with a stepped pin (half of the moving surface) (a). thrust vs. time; b). thrust vs. minimum film thickness). Heavy lines for $h_0 = 20\ \mu m$; dashed lines correspond to $h_0 = 40\ \mu m$; full circles for $v = 1x10^{-3}\ mm/s$; pluses for $v = 1x10^{-2}\ mm/s$; full triangles for $v = 1x10^{-1}\ mm/s$; no symbols for $v = 1\ mm/s$.

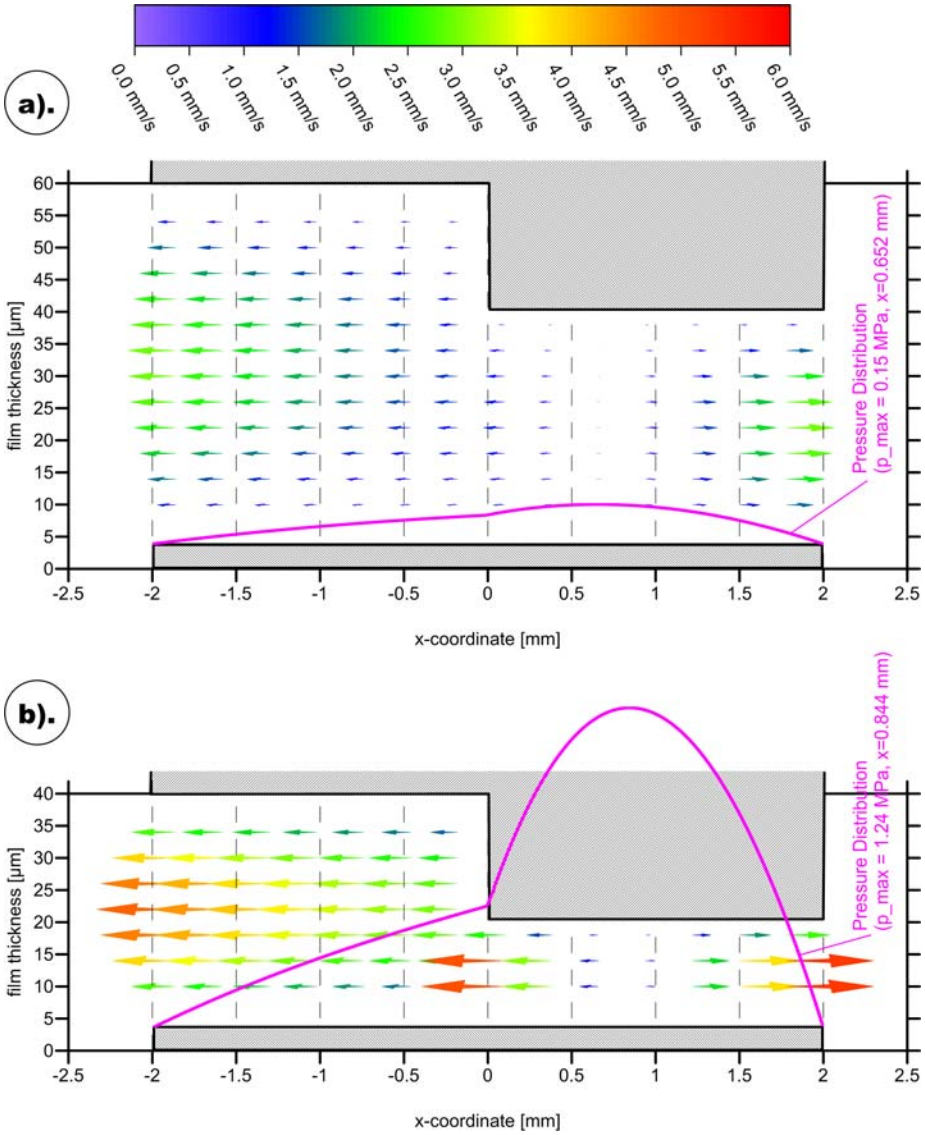

Fig. 4. Velocity profiles and pressure distribution at $z = 0$ symmetry plane
for constant velocity squeeze with $v = 1x10^{-1}$ *mm/s*
(a). $h_0 = 40\ \mu m$, $h = 36\ \mu m$;
b). $h_0 = 20\ \mu m$, $h = 16\ \mu m$)
(clearance exaggerated).

As a note, the lower speeds are more representative for runout. High squeeze speeds are common to impacts or shocks, and the simulation results

confirm that squeeze-film dampers are efficient in absorbing loads. For such machine elements, the energy is dissipated as the lubricant flows after impact.

At higher film thickness, Fig. 4a and Fig. 5, the pressure distribution is more similar to the parabolic distribution of simple parallel plates [2]. When the loading is more extreme, Fig. 4b, the step shifts the high pressure zone to lower film thicknesses. The change in the position of maximum pressure location is also connected with a change of the center of thrust, away from the pin geometrical center, and may lead to stability problems.

When the film thickness diminishes, a change of the pressure gradient around the step is observable, as seen in Fig. 4b, and Fig. 5.

Comparing the pressure distribution on the top and bottom surfaces, only a slight and negligible difference has been found. For this reason, only the lower surface pressure distributions have been presented. The negligible pressure difference between the two surfaces confirms the lubrication hypothesis of constant pressure across the thin film.

Concerning the velocity profiles across the film thickness, Fig. 4a, Fig. 4b and Fig. 5, they are close to the un-stepped parallel plate squeeze-film flow parabolic distributions [2]. The correlation is diminished as the film thickness gets lower, or when the film-squeeze velocity is high.

If the bottom surface pressure field contour plot is superposed on the corresponding velocity profiles of cells just above it is given in Fig. 6, one can see that the fluid is accelerated in the sharp pressure drop region, under the step. The highest speeds are encountered away from the maximum pressure zone, Fig. 4 – 6.

An overview of the bottom surface pressure field for various cases of constant velocity squeeze is given in 3D surface map plots, Fig. 7 and Fig. 8. The highest maximum pressures, Fig. 7 and Fig. 8, can go up to *1.5 MPa*; the value can increase further if the film thickness is lowered or if the squeeze velocity is increased,

The use of sine-profile surface displacement, leading to a sine-profile velocity squeeze, is in fact a particular case of Stephan's problem [12] - the first to observe the "apparent adhesion" of the fluid to the walls. As cited in [7], the "apparent adhesion" appears in cases of no-slip squeeze film flow where motion of the surfaces could take place in either direction.

For sine-wave profile displacement, cavitation was not considered at reverse squeeze to simplify the approach.

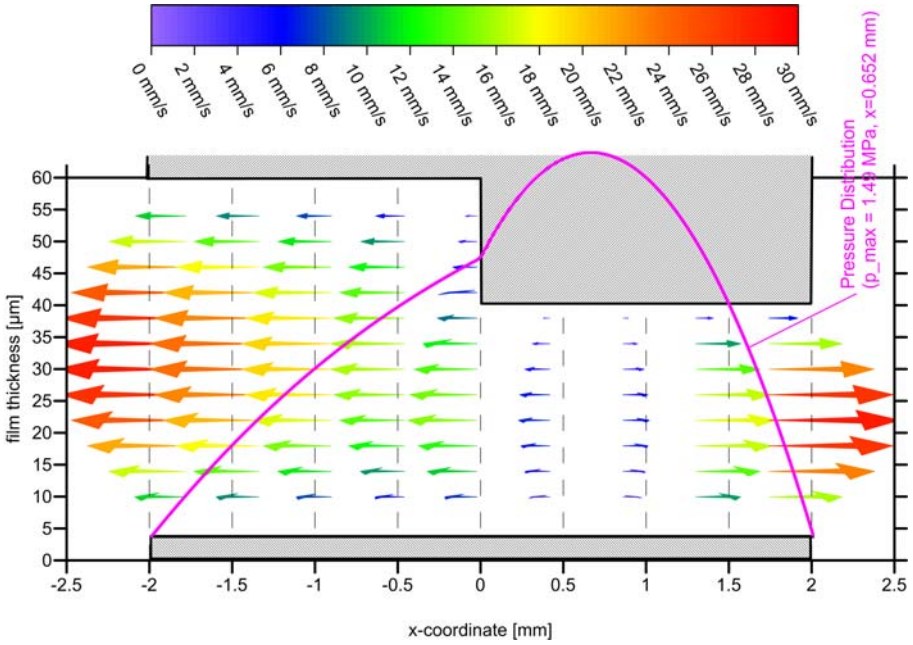

Fig. 5. Velocity profiles and pressure distribution at $z = 0$ symmetry plane for constant velocity squeeze with $v = 1$ *mm/s* ($h_0 = 40$ *μm*, $h = 36$ *μm*) (clearance exaggerated).

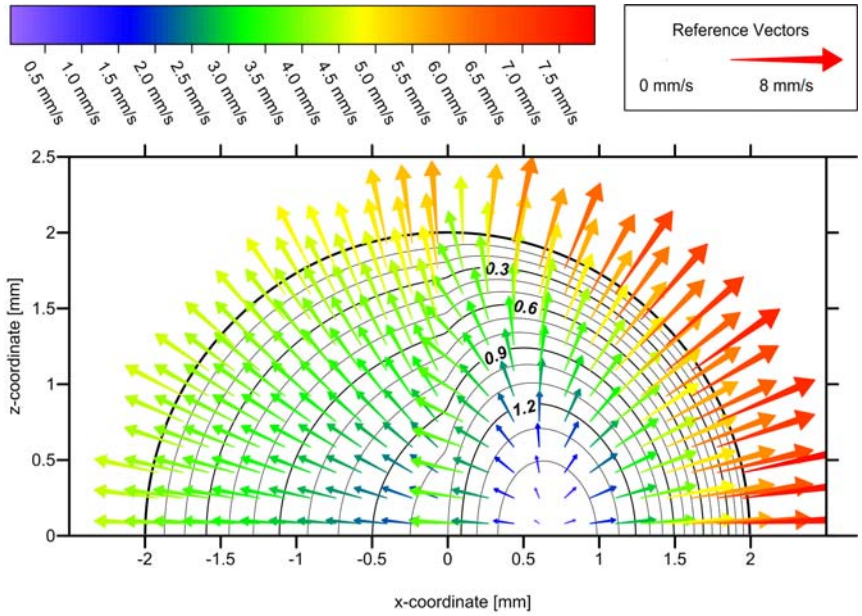

Fig. 6. Velocity profiles and pressure distribution on the moving surface (half) for constant velocity squeeze with $v = 1$ *mm/s* ($h_0 = 40$ *μm*, $h = 36$ *μm*) (isobars [MPa] in black lines).

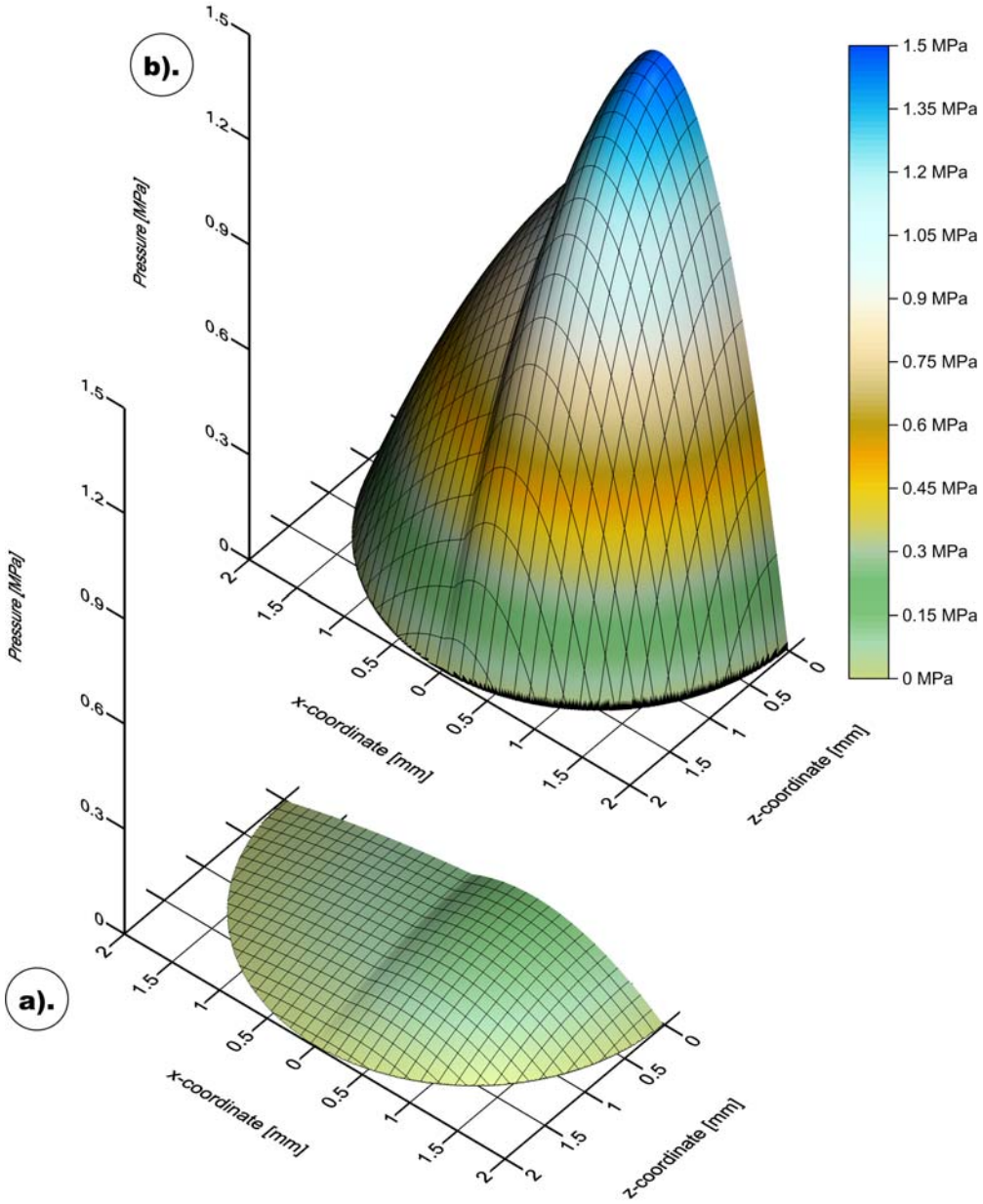

Fig. 7. Pressure distribution on the moving surface (half) for constant velocity squeeze (a). $v = 1x10^{-1}$ *mm/s,* $h_0 = 40$ *μm,* $h = 36$ *μm*; b). $v = 1$ *mm/s,* $h_0 = 40$ *μm,* $h = 36$ *μm*).

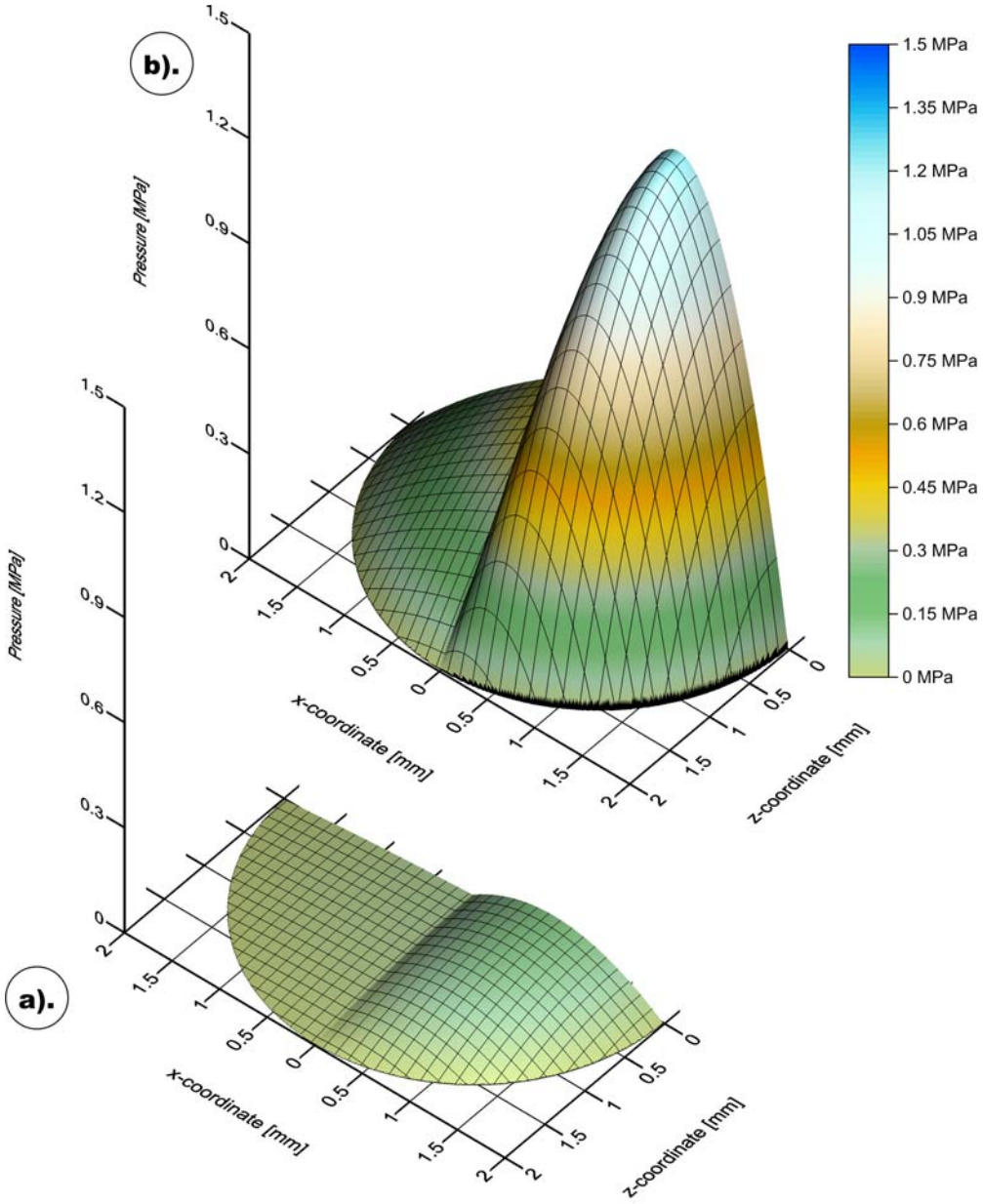

Fig. 8. Pressure distribution on the moving surface (half) for constant velocity squeeze (a). $v = 1x10^{-2}$ *mm/s,* $h_0 = 20$ *μm,* $h = 16$ *μm*; b). $v = 1x10^{-1}$ *mm/s,* $h_0 = 20$ *μm,* $h = 16$ *μm*).

While the problem of choosing a proper time step may not be apparent for constant velocity squeeze, as fluid inertia at small film thicknesses is negligible, one needs an adequate number of points to describe the sine-wave displacement profile. For one of the "extreme" loading cases, high speed with low film thickness; several solutions are presented in Fig. 9. Reducing the number of time steps leads to errors, Fig. 9 zoom. For this reason small time steps, relative to the squeeze velocity, have been used throughout the study for all simulations. Though even smaller time steps would have increased the solution accuracy, the computation time would have increased too much for the current analysis stage.

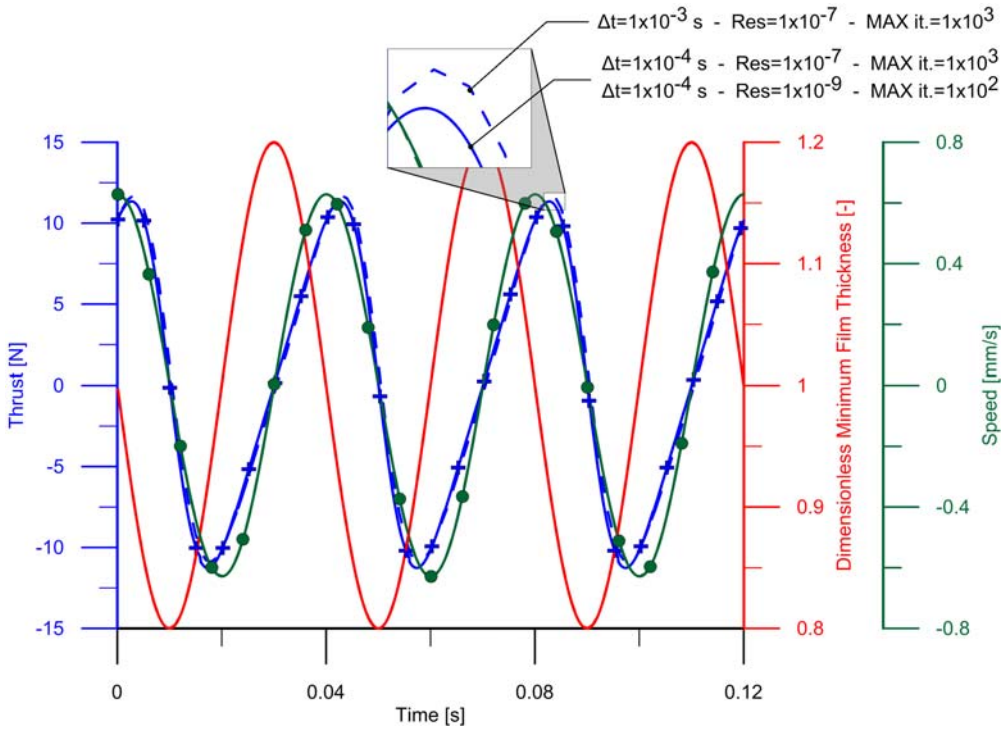

Fig. 9. Theoretical thrust generated at sine-profile velocity squeeze with a stepped pin (half) - Influence of time step and convergence criteria
($h_0 = 20\ \mu m$, $A = 4\ \mu m$, $T = 0.04\ s$, $\omega = 25$ Hz).
Circles for speed curves, plusses for thrust,
no symbols for dimensionless minimum film thickness.

Concerning the residuals, one can see that 10^{-7} convergence stop is sufficient, and in most cases a solution was found in around 100 iterations per time step. A slower convergence was observed for the more refined $h_0 = 40\ \mu m$

mesh compared to $h_0 = 20\ \mu m$, for the same squeeze velocities. Slower convergence on refined meshes is due to the higher number of equations that need to be solved simultaneously for all cells.

Any numerical simulation contains errors at start, hence only the third and final period with smoothened errors have been plotted in Fig. 10 to Fig. 12. Though relatively high thrust is encountered at the fast oscillations, Fig. 10 and Fig. 11, realistic cases for runout defects are between *0.25 Hz* and *2.5 Hz*. Extreme squeeze cases can exceed *2.5 Hz*, but hardly reach *25 Hz.*

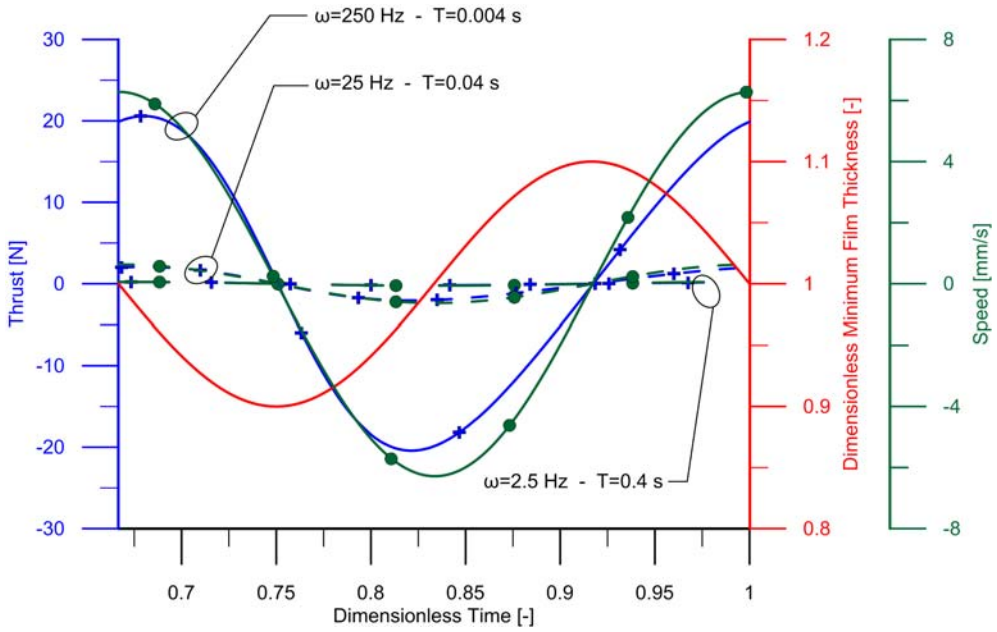

Fig. 10. Theoretical thrust generated at sine-profile velocity squeeze with a stepped pin (half) – Influence of various squeeze profiles – Zoom at the 3rd period of squeeze.
($h_0 = 40\ \mu m$, $A = 4\ \mu m$, $T = 0.004\text{-}0.4\ s$, $\omega = 2.5\text{-}250\ Hz$)
Circles for speed curves, plusses for thrust,
no symbols for dimensionless minimum film thickness.

Examining Fig. 10 to Fig 11, it results that thrust follows more closely the velocity profile sine-wave than the displacement profile. For particular simulation case, the maximum thrust does not occur at the local minimum film thickness, but it is close to the point of maximum velocity. Finally, thrust does not resemble a sine-wave variation, as it depends both on velocity and film thickness.

An analysis of the more frequent loading cases for the two minimum film thicknesses is provided in Fig. 12. For the *4 mm* diameter pin considered herein,

the results at *2.5 Hz* are not negligible. The small drop in thrust around *0.8 dimensionless time*, is caused by cells next to the bottom surface collapse.

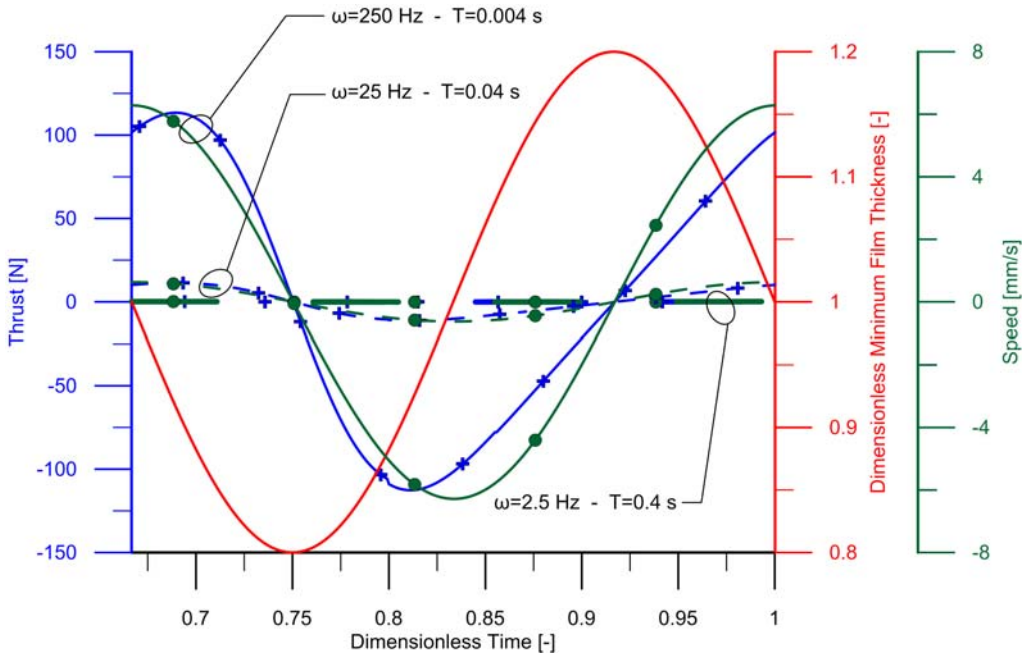

Fig. 11. Theoretical thrust generated at sine-profile velocity squeeze with a stepped pin (half) – Influence of various squeeze profiles – Zoom at the 3rd period of squeeze.
(h_0 = *20 μm, A = 4 μm, T =0.004-0.4 s, ω = 2.5-250 Hz*)
Circles for speed curves, plusses for thrust,
no symbols for dimensionless minimum film thickness.

If surface tension and film rupture had been considered, then the thrust variation would have differed in the case of separating plates. Moreover, if the loading regime is sufficiently high, the fluid could detach entirely from one of the surfaces. Though, such an analysis would require more powerful numerical model based on two-phased flow.

For a real Rayleigh step pin, a change in minimum film thickness affects both squeeze and physical wedge pressure generation mechanisms. By taking into account also the velocity component of the lower surface towards the converging gap, a follow-up study will assess performance of a Rayleigh step pin with runout surface defects considering both pressure build-up mechanisms.

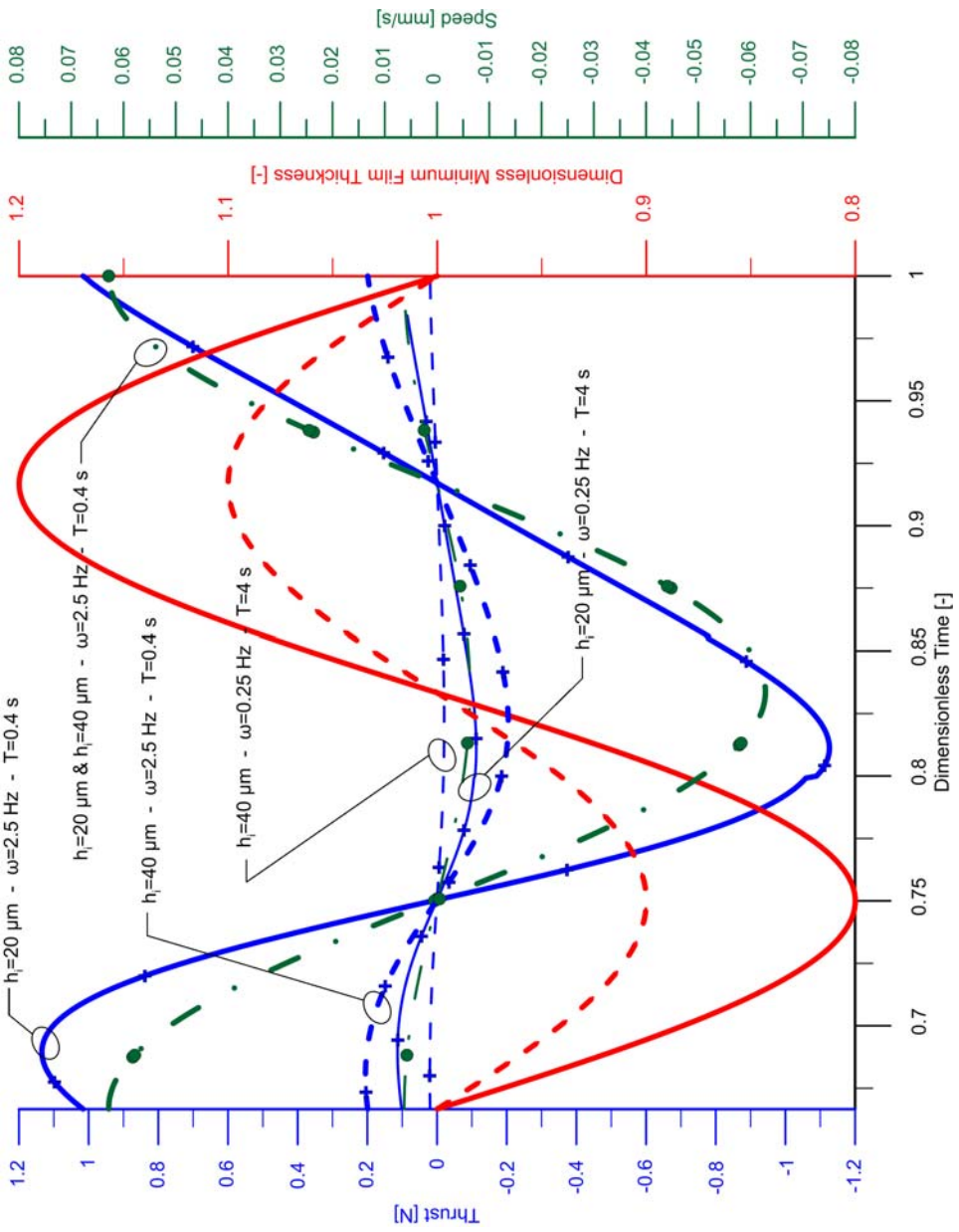

Fig. 12. Theoretical thrust generated at sine-profile velocity squeeze with a stepped pin (half) – Influence of various squeeze profiles and initial clearances – Zoom at the 3rd period of squeeze)
(h_0 = *20 & 40 µm, A = 4 µm, T =0.4 & 4 s, ω = 0.25 & 2.5 Hz*)
Continuous lines for h_0 = *20 µm*; drashed lines for h_0 = *40 µm*; dash-dot lines for squeeze rates.
Circles for speed curves, plusses for thrust,
no symbols for dimensionless minimum film thickness.

4. Conclusions

A numerical investigation has been performed for a stepped pin fully immersed in a viscous Newtonian lubricant undergoing squeeze-film flow as the top and bottom surfaces approach with constant or sine-wave profile velocities. The method is used to characterize a runner-pad with runout, and the emphasis is on the squeeze-film flow effects only.

At high film thicknesses, the influence of the step on the pressure field is smaller than at low film thicknesses. For low film thicknesses and high speeds, the pressure gradient around the step is altered.

For a sine-wave displacement of the surfaces, the resulting thrust follows closely the velocity profile, and a significant phase difference is observed with respect to the surface displacement profile. Aside from a phase difference between maximum thrust and maximum squeeze velocity or minimum film thickness, the resulting thrust does not have a sine-wave shape as it depends both on film thickness and surface velocity.

Neglecting cavitational effects at reverse squeeze leads to unrealistic large downforce values and to anti-symmetrical thrust distributions.

For high velocities a significant amount of thrust is generated, hence squeeze-film flow is efficient to absorb loads and dissipate energy.

Acknowledgements

The work has been funded by the Sectoral Operational Programme Human Resources Development 2007-2013 of the Romanian Ministry of Labour, Family and Social Protection through the Financial Agreement POSDRU/88/1.5/S/60203.

REFERENCES

[1] *M. J. Neale*, The Tribology Handbook (2nd Edition), Butterworth-Heinemann, 1995.
[2] *D. M. Moore*, Viscoelastic Machine Elements: Elastomers and Lubricants in Machine Systems, Butterworth-Heinemann, 1993.
[3] *C. Suciu*, Contributii la studiul amortizoarelor cu frecare fluida pentru controlul vibratiilor (Contributions to the study of squeeze-film dampers for controlling vibrations), PhD dissertation, UPB, Bucharest, 1997. (in Romanian)
[4] *G. W. Stachowiak and A. W. Batchelor*, Engineering Tribology (2nd Edition), Butterworth-Heinemann, 2000.
[5] *D. Coblaş, C. Bălan*, Numerical and experimental analyze of viscous fluids in oscillatory squeezing flow, Mathematical Modeling in Civil Engineering - Scientific Journal, **7** No. 1-2.
[6] *D. Coblaş, D. Broboană, C. Bălan*, Rheological characterization of viscous fluids in oscillatory squeezing flows, Scientific Bulletin" Series D: Mechanical Engineering, **72**, 177-184, 2010
[7] *J. Engmannm*, *C. Servais*, *A. S. Burbidge*, Squeeze flow theory and applications to rheometry: A review, J. Non-Newtonian Fluid Mech., **132**, 1–27, 2005.
[8] *** ANSYS Fluent Theory Guide, 2009.

[9] *M. D. Pascovici*, *A. Predescu*, *T. Cicone* and *C. S. Popescu*, Experimental evidence of cavitational effects in a Rayleigh step slider, Proc. I Mech. E. J **225**, 527-537, 2011.
[10] *A. J. Chorin*, Numerical Solution of the Navier-Stokes Equations, Math. Comp., **22** 104, 756-762, 1968.
[11] *M. Dobrica*, *M. Fillon*, Reynolds' Model Suitability in Simulating Rayleigh Step Bearing Thermohydrodynamic Problems, Tribology Transactions, **48**, 522-530, 2005.
[12] *J .F. Stefan,* Versuche über die scheinbare adhäsion. Sitz. Kais. Akad. Wiss. Math. vol. 69, p. 713-735, 1874.